Journal of Physics B: Atomic, Molecular and Optical Physics

PAPER

Attosecond synchronization of extreme ultraviolet high harmonics from crystals

To cite this article: Giulio Vampa *et al* 2020 *J. Phys. B: At. Mol. Opt. Phys.* **53** 144003

IOP Publishing Journal of Physics B: Atomic, Molecular and Optical Physics
J. Phys. B: At. Mol. Opt. Phys. 53 (2020) 144003 (5pp) https://doi.org/10.1088/1361-6455/ab8e56

Attosecond synchronization of extreme ultraviolet high harmonics from crystals

Giulio Vampa[1], Jian Lu[1], Yong Sing You[1], Denitsa R Baykusheva[1], Mengxi Wu[2], Hanzhe Liu[1], Kenneth J Schafer[2], Mette B Gaarde[2], David A Reis[1] and Shambhu Ghimire[1,3]

[1] Stanford PULSE Institute, SLAC National Accelerator Laboratory, Menlo Park, CA 94025, United States of America
[2] Department of Physics and Astronomy, Louisiana State University, Baton Rouge, LA 70803, United States of America

E-mail: shambhu@slac.stanford.edu

Received 24 January 2020, revised 24 April 2020
Accepted for publication 29 April 2020
Published 17 June 2020

Abstract

The interaction of strong near-infrared (NIR) laser pulses with wide-bandgap dielectrics produces high harmonics in the extreme ultraviolet (XUV) wavelength range. These observations have opened up the possibility of attosecond metrology in solids, which would benefit from a precise measurement of the emission times of individual harmonics with respect to the NIR laser field. Here we show that, when high-harmonics are detected from the input surface of a magnesium oxide crystal, a bichromatic probing of the XUV emission shows a clear synchronization largely consistent with a semiclassical model of electron–hole recollisions in bulk solids. On the other hand, the bichromatic spectrogram of harmonics originating from the exit surface of the 200 μm-thick crystal is strongly modified, indicating the influence of laser field distortions during propagation. Our tracking of sub-cycle electron and hole re-collisions at XUV energies is relevant to the development of solid-state sources of attosecond pulses.

Keywords: high harmonics, coherent control, extreme ultraviolet

Supplementary material for this article is available online

(Some figures may appear in colour only in the online journal)

1. Introduction

Generation of extreme ultraviolet (XUV) high harmonics from gaseous media has been the foundation of attosecond science [1, 2], which includes attosecond pulse generation [3], imaging molecular orbitals [4] and attosecond tunneling interferometry [5, 6]. At the heart of atomic high-order harmonic generation (HHG) lies a three-step recollision process [7] that consists of tunnel ionization, free-electron acceleration, and recollision to the parent ion. Based on their kinetic energies, electrons recollide with the parent ions at slightly different times in the subcycle scale [8], causing an intrinsic delay between harmonics. This delay, termed 'atto-chirp', is deleterious for crafting transform-limited isolated attosecond pulses or attosecond pulse trains. The precise timing between the electron trajectories is the cornerstone of high-harmonic spectroscopy [5]. Following the recent observation of high-harmonic emission from bulk crystals [9–17], attosecond metrology is being extended to solids, with methods developed to reconstruct electronic band structures in reciprocal space [14, 18], to probe the periodic potential in real space [16, 17], and to boost the emission efficiency in nano-structures [19–22], as well as toward stable attosecond pulses [23]. Just like in gas-phase HHG, many of these applications benefit from the understanding of the temporal connection between harmonics and the driving NIR laser field at the sub-cycle level.

[3] Author to whom any correspondence should be addressed.

In solids, there are two major HHG channels and they are expected to have distinct temporal profiles [24]. XUV harmonics from thin SiO_2 subjected to NIR laser fields were found chirp-free [14, 25], which is consistent with Bloch-like nonlinear oscillations of electrons in the conduction bands. The other competing channel is inter-band polarization or recollision based harmonics [13, 24, 26, 27], similar to HHG from gases. As shown in ultraviolet harmonics from ZnO, this process preserves the temporal mapping characteristic of gas-phase HHG [13]. In MgO crystals, the modulation of the high-harmonic spectrum with the carrier-envelope phase of the few-cycle laser pulse [28], as well as the laser-intensity-induced shift in the emission phase of individual harmonics [29] also point toward the inter-band or recollision-based emission, however the atto-chirp has not been measured.

Here we apply a bichromatic probing scheme [5, 6, 8, 13] to XUV high-harmonics emitted from the input and exit surfaces of a magnesium oxide crystal. Harmonics emitted from the input surface show clear spectral signatures consistent with recolliding electron–hole pair trajectories, and quantify the 'atto-chirp'. This is our first result. Spectrograms of harmonics emitted from the exit surface of a 200 micrometer thick MgO, however, are strongly distorted. This is our second result. Together with a measured broadening and blue-shift of the transmitted NIR spectrum, we conclude that the bichromatic probing scheme encodes temporal nonlinearities experienced by the NIR pump during propagation through the crystal. Spatial distortions of the XUV high-harmonic beam from the same crystal has been recently reported, too [30]. Lastly, we develop a quantum-mechanical model of high-harmonic generation in solids that adds tunneling of the electron–hole pair across the minimum bangap of MgO. Implications of our work include the possibility of developing attosecond metrologies based on recolliding electrons at XUV photon energies in solids and the generation of attosecond pulses with crystals.

2. Experiment

In the experiment, we measure high harmonics from MgO crystals with 200 μm thickness subjected to an NIR field centered at 1320 nm and its weak second harmonic. Both the fundamental and second harmonic are polarized along the [100] direction of the crystallographic axis. We record the XUV high-harmonic spectra as a function of the attosecond delay between the two colors, which is controlled with a pair of glass wedges (see the supplementary material for more detail, which can be found online at https://stacks.iop.org/JPB/53/mmedia).

We begin our investigation by showing the relevance of temporal distortions of the infrared field upon propagation. This is performed by comparing two-color driven harmonic spectra in the transmission mode (figure 1, top panel) with those in the reflection mode (figure 1, bottom panel), but otherwise under similar conditions (see supplementary information for details). The excitation intensity inside the sample in both cases (considering Fresnel loss) is estimated to be $\sim$10 TW cm^{-2}. Because XUV harmonics are effectively emitted within a thickness that is on the order of one absorption length ($\sim$10 nm), from the entrance side in the reflection geometry and from the exit side in the transmission geometry, the transmitted harmonics are expected to encode the distortions accumulated by the pump pulse during propagation from the entrance to the exit side of the sample. Indeed, transmitted harmonics exhibit broader peaks, which we attribute to the broader (by about 30 percent) and blue-shifted spectrum of the fundamental pulse upon propagation (see supplementary information). Moreover, each individual transmitted harmonic exhibits a linear frequency shift with the second harmonic delay (shown by the dashed line), which is consistent with different NIR center frequencies across the pulse. Spectral broadening and frequency shifts are a result of nonlinear propagation effects, possibly self-phase modulation, since no frequency shift on individual harmonics is measured in reflection mode (dashed line). Linear dispersion of MgO is ruled out as a possible contribution by adding a similarly thick MgO crystal in the beam path before the focusing lens, for the reflection geometry.

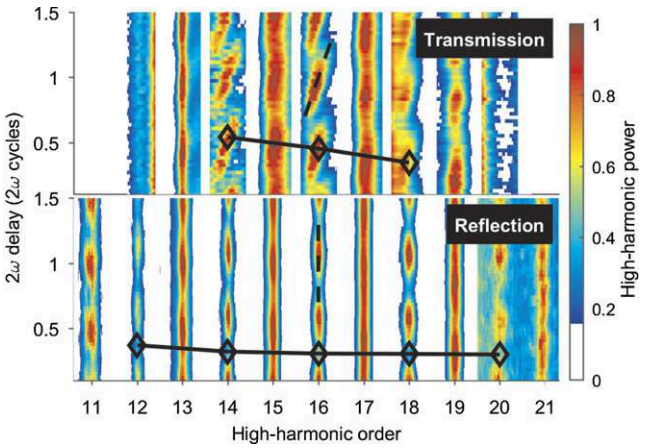

Figure 1. The modulation of the even harmonics measured in the transmission geometry (top panel) shows an intra-harmonic chirp (dashed black line), resulting in inconsistent determination of the modulation phase. Unequivocal determination of the modulation phase is possible, instead, in the reflection geometry–here set at a 45° angle of incidence (bottom panel). The local minima for the even-harmonic modulation are extracted and indicated by the diamond symbols. Each harmonic is independently normalized to 1.

In addition to the individual frequency shifts, there is a delay across neighboring harmonics. As shown in a previous work [8], this modulation provides a measurement of the sub-cycle emission time of the harmonics, the so-called 'atto-chirp'. This quantity is derived by matching the observed modulation with that predicted by a model of recolliding electron–hole pairs in MgO, as described in the next paragraph and in the supplementary information. In the reflection geometry, we measure a lower limit for the attochirp decreasing from 148 ± 44 as/eV at $\sim$ 11 eV to 11 ± 44 as/eV at $\sim$ 15 eV, when a semiclassical model of recolliding electron–hole pairs is considered. The atto-chirp deduced with a quantum model (described below) is compatible with the semiclassical one, but has a larger uncertainty (supplementary figure 4). The phase of the inter-harmonic modulation is stronger in the transmission geometry, but the marked intra-harmonic shift renders determination of this phase inconsistent.

Next, we analyze the observed modulation of the even-order harmonics as a function of the two-color delay in detail,

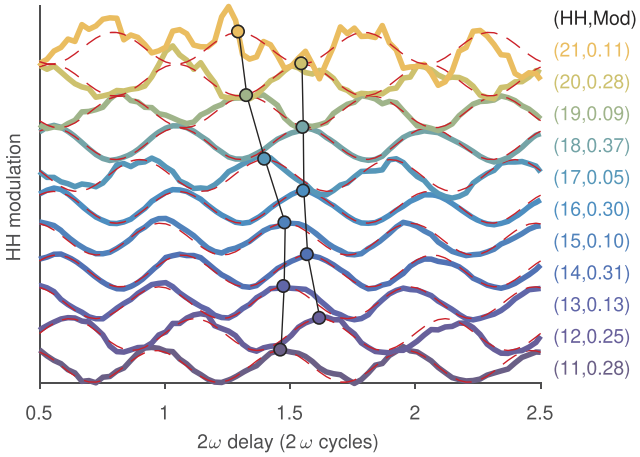

Figure 2. Modulation of high-harmonic power for harmonics 11th to 21st (color coded) versus sub-cycle delay between the fundamental and second harmonic fields (in cycles of the second harmonic) measured in the reflection geometry. The order of the harmonic and the modulation amplitude (normalized to 1) are reported in parentheses next to the curves on the right-hand side. The delay that yields the highest power is marked by colored circles for every harmonic. The dashed red lines are fits to the experimental modulation with function $\cos(\phi + \phi_{opt})$, where ϕ is delay. The only fit parameter is the offset phase, ϕ_{opt}. The second harmonic power is set to ∼0.5% of the fundamental, which is estimated to correspond to ∼1% of the fundamental intensity (see supplementary information).

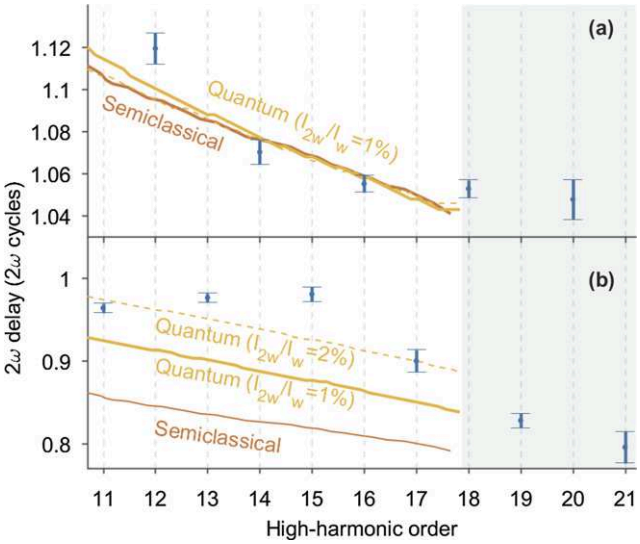

Figure 3. (a) Both the semi-classical and quantum correction models of recolliding electron–hole pairs predict a harmonic order dependent phase for the modulation of the even-order harmonics. They closely match the experimental data (blue markers), up to an offset (see supplementary information for details). This is the so called 'atto-chirp'. The odd harmonics (panel b) also show order dependence but they deviate significantly from the model. The deviation decreases for increasing intensity of the second harmonic (dashed line), but still falls short of predicting the maximum at the 15th order. The predictions from the model are restricted within the maximum band-gap at the zone edge. The 18th and 21st harmonics lie above the maximum band-gap, indicated by the gray area.

for the reflection geometry. When a second harmonic field with ∼1% of the intensity of the pump is added to the fundamental driver and properly phased, the asymmetric field breaks the inversion symmetry of the high-harmonic dipole, resulting in electrons and holes being accelerated farther apart or closer together at subsequent laser half-cycles of the driver. The uneven path length is described by the addition or subtraction of a phase $\sigma(n\omega, \phi)$ to the oscillating high-harmonic dipole [8, 13], dependent on the harmonic order n and two-color delay ϕ (see supplementary information). As the delay ϕ is varied, the high-harmonic power modulates with an order-dependent phase. This is shown in figure 2 for the reflection case.

Experimental parameters are reported in the supplementary information. The delay that yields the highest harmonic power (ϕ_{opt}) is extracted from a cosine fit of the normalized modulations with a fixed frequency for all harmonics. It is plotted in figure 2 (colored circles) for the even and the odd harmonics separately, and in figure 3, where it is compared with the theoretical predictions. Overall, the delay for the even harmonics agrees reasonably well with the simple semiclassical three-step model introduced above (orange line) [26, 27], up to an unmeasured offset phase. In essence, the agreement suggests that XUV harmonics from MgO are a result of recollisions between electrons and their associated holes that are driven by the strong laser fields in the lowest conduction and one of the highest valence bands, respectively. The measured attochirp is consistent with so-called *short trajectories*. It is possible that *long trajectories* are suppressed due to spatio-temporal averaging across the laser focus, unfavorable transverse phase matching, or rapid decoherence. The latter may be due to many-body interactions during the laser-driven excursion, or to spatial inhomogeneities probed by the potentially extended wavepacket [31]. Bloch-like emission, instead, predicts a modulation phase which is either in-phase or out-of-phase with the second harmonic delay, but without atto-chirp (see derivation in the supplementary information). We note that the semiclassical model predicts the emission phase of harmonics only up to 18th order because of the limit set by the maximum band-gap at the zone edge. The emission of harmonics beyond this order would require considerations of tunneling to a higher-lying conduction band [28, 32, 36] although experimental data does not show any apparent abrupt changes in the emission phase around this energy range. Harmonics between 18th–21st (included) lie in the bandgap with the second conduction band [33].

We note that the semiclassical model neglects quantum aspects similar to those studied both theoretically [34] and experimentally [6] in the gas phase. Here, we extend those calculations to the solid-state platform for the first time (see derivation in the supplementary information), see yellow line figure 3(a). However, the difference is not statistically significant and is within the uncertainty in the extracted phase for otherwise fixed model parameters. The theoretical framework that we have developed for solids predicts an imaginary component of the birth time of about 460 as for harmonics in the photon energy range from 12 eV to 18 eV (supplementary figure 3), corresponding to ∼ 0.1 cycles of the NIR field. This value is similar to that measured in He atoms driven at 4.4 $\times 10^{14}$ W cm^{-2} [6]. However, we find a large offset of the

modulation phase for the odd harmonics, compared to both the semiclassical model and that with this extended model (figure 3(b)). The offset decreases assuming a stronger second harmonic, thus suggesting an underestimate of the experimental field strength, but the model falls short of predicting the maximum at the 15th harmonic. The large deviation might arise from physics beyond our model. Supplementary figure 5 confirms, with additional experimental data, that for increasing second-harmonic strength the relative modulation phase for even versus odd harmonics progressively decreases. A flattening in the relative phase of the even harmonics is observed as the second harmonic strength increases to 0.56% of the fundamental. Therefore, the reported atto-chirps shall be considered lower limits.

3. Conclusions

In conclusion, we measured the attosecond synchronization of XUV harmonics from 200 micrometer thick MgO crystals subjected to intense NIR laser fields. The results obtained in the reflection geometry closely represent the intrinsic delay of high-harmonics predicted by generalized re-collision model, whereas two-color spectrograms of harmonics measured in the transmission geometry show strong temporal distortions–a cautionary tale for performing *in-situ* high-harmonic spectroscopy in this geometry. Our evidence suggests that they are strongly influenced by propagation effects. In the reflection geometry, using semiclassical trajectories we extract a minimum atto-chirp of 11 ± 44 as/eV (lower limit) about the 16th harmonic at $\sim$15 eV. With proper dispersion compensation, such as with ultra-thin metal filters, XUV harmonics from MgO could support attosecond pulse trains. Typical gas-phase harmonic sources operate at about two orders of magnitude higher laser intensities. Because of the modest peak intensity requirements, solid-state HHG based sources should be feasible with modern high repetition rate laser systems [35] such that the total XUV flux can be increased significantly.

Author contributions

SG conceived the experiments. JL conducted experiments, GV performed calculations. GV and JL contributed equally to this work. YSY conducted initial measurements. MW and DB also performed independent calculations. HL helped in initial measurements. All authors contributed to the interpretation of the results and writing of the manuscript.

Acknowledgments

At Stanford/SLAC, this work was primarily supported by the US Department of Energy, Office of Science, Basic Energy Sciences, Chemical Sciences, Geosciences, and Biosciences Division through the Early Career Research Program. GV acknowledges the support from W M Keck Foundation. DB acknowledges the support from the Swiss National Science Foundation (SNSF) through project number P2EZP2-184255. The work at LSU was supported by the National Science Foundation (NSF) (PHY-1713671). The authors declare that they have no competing financial interests.

ORCID iDs

Giulio Vampa https://orcid.org/0000-0001-8492-3408

References

[1] Corkum P B and Krausz F 2007 Attosecond science *Nat. Phys.* **3** 381
[2] Krausz F and Ivanov M 2009 Attosecond physics *Rev. Mod. Phys.* **81** 163
[3] Paul P M *et al* 2001 Observation of a train of attosecond pulses from high harmonic generation *Science* **292** 1689–92
[4] Itatani J *et al* 2004 Tomographic imaging of molecular orbitals *Nature* **432** 867
[5] Shafir D *et al* 2012 Resolving the time when an electron exits a tunnelling barrier *Nature* **485** 343
[6] Pedatzur O *et al* 2015 Attosecond tunnelling interferometry *Nat. Phys.* **11** 815–9
[7] Corkum P B 1993 Plasma perspective on strong field multiphoton ionization *Phys. Rev. Lett.* **71** 1994
[8] Dudovich N *et al* 2006 Measuring and controlling the birth of attosecond XUV pulses *Nat. Phys.* **2** 781
[9] Ghimire S *et al* 2011 Observation of high-order harmonic generation in a bulk crystal *Nat. Phys.* **7** 138
[10] Schubert O *et al* 2014 Sub-cycle control of terahertz high-harmonic generation by dynamical Bloch oscillations *Nat. Photon.* **8** 119
[11] Ndabashimiye G *et al* 2016 Solid-state harmonics beyond the atomic limit *Nature* **534** 520
[12] Hohenleutner M *et al* 2015 Real-time observation of interfering crystal electrons in high-harmonic generation *Nature* **523** 572
[13] Vampa G *et al* 2015 Linking high harmonics from gases and solids *Nature* **522** 462
[14] Luu T T *et al* 2015 Extreme ultraviolet high-harmonic spectroscopy of solids *Nature* **521** 498
[15] Garg M *et al* 2016 Multi-petahertz electronic metrology *Nature* **538** 359
[16] Liu H *et al* 2017 High-harmonic generation from an atomically thin semiconductor *Nat. Phys.* **13** 262
[17] You Y S, Reis D A and Ghimire S 2017 Anisotropic high-harmonic generation in bulk crystals *Nat. Phys.* **13** 345
[18] Vampa G *et al* 2015 All-optical reconstruction of crystal band structure *Phys. Rev. Lett.* **115** 193603
[19] Han S *et al* 2016 High-harmonic generation by field enhanced femtosecond pulses in metal-sapphire nanostructure *Nat. Commun.* **7** 13105
[20] Sivis M *et al* 2017 Tailored semiconductors for high-harmonic optoelectronics *Science* **357** 303–6
[21] Vampa G *et al* 2017 Plasmon-enhanced high-harmonic generation from silicon *Nat. Phys.* **13** 659
[22] Liu H *et al* 2018 Enhanced high-harmonic generation from an all-dielectric metasurface *Nat. Phys.* **14** 1006
[23] Garg M, Kim H-Y and Goulielmakis E 2018 Ultimate waveform reproducibility of extreme-ultraviolet pulses by high-harmonic generation in quartz *Nat. Photon.* **12** 291–6
[24] Wu M, Ghimire S, Reis D A, Schafer K J and Gaarde M B 2015 High-harmonic generation from Bloch electrons in solids *Phys. Rev.* A **91** 043839

[25] Luu T T and Wörner H J 2018 Observing broken inversion symmetry in solids using two-color high-order harmonic spectroscopy *Phys. Rev.* A **98** 041802
[26] Vampa G *et al* 2014 Theoretical analysis of high-harmonic generation in solids *Phys. Rev. Lett.* **113** 073901
[27] Vampa G, McDonald C, Orlando G, Corkum P and Brabec T 2015 Semiclassical analysis of high harmonic generation in bulk crystals *Phys. Rev.* B **91** 064302
[28] You Y S *et al* 2017 Laser waveform control of extreme ultraviolet high harmonics from solids *Opt. Lett.* **42** 1816–9
[29] Lu J, Cunningham E F, You Y S, Reis D A and Ghimire S 2019 Interferometry of dipole phase in high harmonics from solids *Nat. Photon.* **13** 96–100
[30] Vampa G, You Y, Liu H, Ghimire S and Reis D 2018 Observation of backward high-harmonic emission from solids *Opt. Express* **26** 12210–8
[31] Yue L and Gaarde M B 2020 Imperfect recollisions in high-harmonic generation in solids *Phys. Rev. Lett.* **124** 153204
[32] You Y S, Lu J, Cunningham E F, Roedel C and Ghimire S 2019 Crystal orientation-dependent polarization state of high-order harmonics *Opt. Lett.* **44** 530–3
[33] Wu M *et al* 2017 Orientation dependence of temporal and spectral properties of high-order harmonics in solids *Phys. Rev.* A **96** 063412
[34] Smirnova O and Ivanov M 2014 *Multielectron High Harmonic Generation: Simple Man on a Complex Plane* (New York: Wiley) ch 7 pp 201–56
[35] Gholam-Mirzaei S, Beetar J and Chini M 2017 High harmonic generation in zno with a high-power mid-ir opa *Appl. Phys. Lett.* **110** 061101
[36] Uzan A J *et al* 2020 Attosecond spectral singularities in solid-state high-harmonic generation *Nat. Photon.* **14** 183–7